Journal of Materials Chemistry C

ROYAL SOCIETY OF CHEMISTRY

PAPER

View Article Online
View Journal | View Issue

Cite this: J. Mater. Chem. C, 2025, 13, 18751

Environmental effects on the electronic states of MoS_2 flakes probed by micro-ARPES

Dario Marchiani, †[a] Marta Pennese, †[a] Nuria Jimenez-Arevalo, [a] Maria Grazia Betti, *[a] Riccardo Frisenda, *[a] José Avila, [b] Pavel Dudin [b] and Carlo Mariani *[a]

Received 3rd April 2025,
Accepted 25th July 2025

DOI: 10.1039/d5tc01402f

rsc.li/materials-c

A spatially resolved angle-resolved photoelectron spectroscopy investigation at the micron scale reveals the effects of the external environment on exfoliated MoS_2 multilayers. The electronic band dispersion and related parameters were measured on MoS_2 samples that were exfoliated and transferred in a controlled air-free atmosphere. Notably, these samples exhibited a more defined band structure and a higher spectral density of states compared to those prepared and transferred in air. In the latter case, surface contamination resulted in band broadening, particularly in the density of states linked to out-of-plane orbitals in the low binding energy region near the valence band maximum. Slight p-doping is also observed for the non-protected sample, which can be associated with tiny effects of ambient oxygen during transport. These findings underscore the necessity of air-protected exfoliation and transfer to accurately capture the fundamental properties of transition metal dichalcogenides.

Introduction

Transition metal dichalcogenides (TMDs) have garnered significant interest due to their attractive properties, which depend on the specific material and layer thickness.[1] These materials are two-dimensional (2D) compounds characterized by an in-plane projected honeycomb lattice and van der Waals (vdW) interactions between stacked layers, with each layer consisting of a three-atom-thick structure. Notably, the interplay between in-plane localized and out-of-plane electronic states[1] allows TMDs to transition from an indirect to a direct band-gap material when their thickness is reduced from multiple layers to a single layer (1L) configuration,[2–4] making them promising candidates for optoelectronic applications.

The optical and electronic properties of transition metal dichalcogenides are highly sensitive to external perturbations, including charge doping, defects,[5] grain boundaries,[6] strain,[7,8] ageing under ambient conditions,[9] oxidation, and adsorbed atoms or molecules. Identifying which perturbations are active in a specific sample remains a significant challenge, posing barriers to optimizing the preparation of these atomically thin materials.

Encapsulation using metal oxide layers, hexagonal boron nitride (hBN),[10] or polymers,[11] offers a strategy to shield TMD flakes from environmental effects, preventing adsorbates and charge traps from degrading carrier mobility. While these methods are effective for various device applications, achieving fine control of the interrelationship between the content of defects/adsorbates/ageing and the optical and electronic properties remains an open question, particularly when comparing ideal semiconducting TMDs to exfoliated flakes prepared in air. In particular, when encapsulation is incompatible with experimental surface-sensitive techniques or with applications that require exposed surfaces.

Molybdenum disulfide (MoS_2) can be considered as the prototype of TMDs, and in its stable bulk form it presents an AB stacking with subsequent layers rotated by 180° (2H-MoS_2). The valence band maximum (VBM) in bulk MoS_2 is located at the Γ point of the hexagonal Surface Brillouin Zone (SBZ) and primarily originates from the out-of-plane Mo $3d_{z^2-r^2}$ and S p_z orbitals. In contrast, the conduction band minimum (CBM) is positioned at the K point and consists of in-plane Mo-associated $d_{x^2-y^2}$ and d_{xy} orbitals. This electronic structure results in an indirect band gap of approximately 1.3 eV.[4] A benchmark technique for determining and evaluating the effects of the external perturbation on the electronic band structure and dispersion of MoS_2 is angle-resolved photoelectron spectroscopy (ARPES).[4,12] High-quality crystalline flakes, typically several tens of micrometres in size, can be obtained *via* exfoliation due to the weak van der Waals interactions between stacked layers. However, for accurate surface electronic structure investigations, sample cleaning is an essential requisite. Full in-ultra-high-vacuum cleavage of van der Waals 2D materials and transfer to the electron

[a] Dipartimento di Fisica, Università di Roma "La Sapienza", Piazzale Aldo Moro, I – 00185 Roma, Italy. E-mail: maria.grazia.betti@roma1.infn.it, carlo.mariani@uniroma1.it, riccardo.frisenda@uniroma1.it
[b] Synchrotron SOLEIL, L'Orme des Merisiers, Départementale 128, Saint-Aubin F – 91190, France
† These authors contributed equally to this paper.

spectroscopy stage is the best method so far for avoiding surface contamination,[13,14] and also capping with a single graphene layer, as used for a metallic TMD.[15] However, the previous methods require non-trivial custom equipment of sample holders and apparatus in order to reach few-layer flakes, which is not always available in different laboratories. Another possible method of surface cleaning is in-vacuum annealing,[4] however this procedure carries the risk of sulphur depletion, as previously observed and quantified,[16] that needs to be healed by exposure to a S source under special conditions.[17] Another viable method is the cleavage and transport *via* a controlled atmosphere, as recently exploited for black phosphorus flakes.[18] Since flake exfoliation is the most widely used, generalised and reproducible preparation method to bring 2D cleavable crystals across different laboratories,[19,20] we adopt this latter cheap, reliable and risk-free approach for accurately investigating the surface electronic properties of TMDs and in general for cleavable 2D materials.

In this study, we systematically analyse the valence band of MoS_2 flakes using μ-ARPES, comparing samples prepared under ambient conditions or in a controlled atmosphere. Our findings highlight the importance of maintaining a controlled environment throughout all stages of sample preparation – from exfoliation and transfer to a photoemission chamber to the μ-ARPES experiment under ultra-high vacuum (UHV) conditions – to prevent spectral artifacts that could affect the surface electronic properties of MoS_2. This approach establishes a viable, cost-effective, and reproducible method for the spectroscopic study of exfoliated TMD flakes, minimising external perturbations.

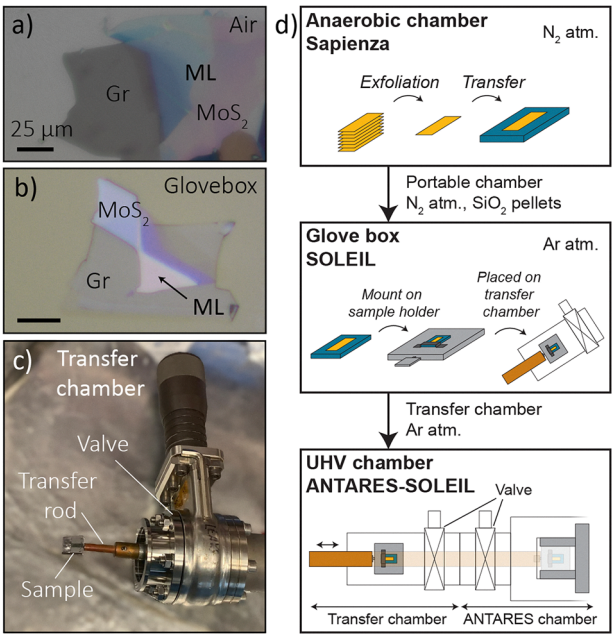

Fig. 1 (a) and (b) Microscopy photographs of air and glove box fabricated multilayer MoS_2 on graphite samples. (c) Photograph of a sample mounted in the transfer chamber taken inside the glove box at SOLEIL. (d) Schematic drawing of the fabrication and transfer process for the glove box sample.

Experimental

A Sample preparation

The MoS_2 flake was deposited onto a graphite multilayer on top of a Pt-coated SiO_2/Si wafer mounted on a Ta sample holder. The graphite and MoS_2 flakes were mechanically exfoliated from natural graphite (ProGraphite GmbH) and molybdenite mineral crystals (Moly Hill mine, Canada), respectively, with Nitto tape (Nitto SPV 224) and then transferred onto the Gel-film (Gel-Pak, WF 4 × 6.0 mil), which is a commercially available polydimethylsiloxane (PDMS) substrate. First, a graphite flake was transferred onto the substrate, later a MoS_2 flake was transferred on top of the graphite flake by deterministic transfer method.[21,22] The air and glove box samples were, respectively, fabricated in air and in a gloveless anaerobic chamber (Bactronez).[23] Optical microscopy photographs of the fabricated samples are shown in Fig. 1a and b, where the bottom graphite flakes and the top MoS_2 can be observed. After fabrication, the air-prepared sample (Fig. 1a) was directly mounted on the sample holder and inserted into the ANTARES UHV chamber. On the other hand, the glove box sample (Fig. 1b) exfoliated and fabricated in a N_2 (99.999% purity) atmosphere was sealed in a portable high-vacuum-sealed chamber filled with N_2 and dry Silica gel for transfer between the laboratory in university La Sapienza and synchrotron SOLEIL. Subsequently, at synchrotron SOLEIL it was opened in a glove box (Jacomex) under an Ar atmosphere (99.999% purity). The protected sample was mounted on the ANTARES sample holder and loaded in the ANTARES transfer chamber (see Fig. 1c). Eventually, the transport chamber was attached to the ANTARES load-lock, then evacuated and transferred into the UHV chamber of the ANTARES instrument. The whole process of the air-protected sample preparation and transfer steps, which lasts less than 1 hour, is schematically depicted in Fig. 1d.

B Micro-ARPES experiment

The μ-ARPES experiment was conducted at the ANTARES beamline of the SOLEIL Synchrotron radiation facility (Saint-Aubin, France). The excitation was given by linearly horizontal polarized photons of 95 eV and the emitted photoelectrons were analysed for energy and angle using a hemispherical electron analyser with a vertically confining entrance slit to allow band mapping (A-1 Analyzer, MB Scientific AB). The scanning photoemission microscope is equipped with Fresnel zone plates for beam focusing, ensuring spatial resolution better than 0.7 μm. Angle-integrated photoemission data were obtained with 200 eV of pass energy, and angle-resolved data were obtained at high energy- and spatial-resolution, with 100 eV of pass energy. During the measurements the sample was kept at a low temperature (90 K), to avoid any possible beam damage.

Results and discussion

The MoS_2 flakes, obtained by cleaving a bulk crystal, are prepared either in air or in a nitrogen-filled glove box, as described in the Experimental section. After preparation, they are imaged using an optical microscope, as shown in Fig. 1a and b. The MoS_2 flakes

present multilayer regions with a linear size of tens of μm. Due to the opacity and the presence of colours due to thin film interference, the multilayer (ML) regions are reasonably thicker than 20 nm. Both samples were transferred to the load-lock in the ultra-high-vacuum chamber of the μ-ARPES system spatially resolved at the micron scale of the ANTARES beamline, as detailed previously. In particular, for the protected-prepared one, the whole process ensured heavily reduced surface contamination. The photoemission extended valence band spectral density, integrated over approximately 0.3 $Å^{-1}$ (a consistent fraction of the surface Brillouin zone in the ΓK direction) around the Γ point and acquired using 95 eV photons, is shown in Fig. 2 (left panel). The energy distribution curves (EDCs) for both the air-prepared (sample A) and glove-box protected (sample B) crystals exhibit a similar overall spectral shape. However, sample A displays significantly broader features, particularly in the lower binding energy (BE) region. In contrast, the glove-box protected sample reveals sharper bands at approximately 2.2, 3.8, and 7.2 eV BE. The two lower-BE peaks can be attributed to hybridized out-of-plane Mo $3d_{z^2-r^2}$ and S p_z orbitals, as predicted for MoS_2 and other TMDs.[1,24] Analogous out-of-plane orbital association has been investigated by ARPES and confirmed by DFT calculations for WTe_2,[15] while the higher BE feature exhibits a predominantly sulphur character,[25] in accordance with increased spectral density due to its higher photo-ionization cross-section at this photon energy.[26] Out of plane orbitals associated with the bands close to the VBM are more sensitive to external perturbations and surface contamination.

Angle-resolved EDCs obtained at high energy resolution taken at the Γ point of the surface Brillouin zone, focusing on the energy region associated with out-of-plane orbitals more sensitive to surface interactions, are presented in Fig. 2b and c. These angle-resolved EDCs clearly emphasize the main differences between the air-exposed sample (A) and the glove-box/vacuum-maintained sample (B). Specifically, sample A shows an overall broadening of the spectral features, while sample B exhibits much sharper and well-defined features. Notably in sample B, instead of the broad continuum of spectral density of states, a finite number of discrete bands are resolved in the ~1–2 eV BE region, suggesting a quantization effect along the *z*-axis. A finite number of discrete 2D states have been recently observed in MoS_2 and other TMDs, attributed to the mechanical isolation of few-layer blocks away from the 3D bulk single crystal.[27] We can thus reasonably associate the presence of these discrete split electronic bands with enhanced interlayer stacking in few-layer planes, which causes the electronic state confinement into discrete few-layer blocks along *z*.[27] An analytical estimation of the observed discrete levels leads to approximately 5–6 electronic bands that can be singled out, corresponding to the same number of blocks of layers. We underline how these discrete bands are uniform in the surface plane across different areas of the same flake.

In order to gain further insight into the band structure, μ-ARPES data were acquired with a zone-plate focused on μm-scale regions of both crystalline flakes. The electronic band structures in the low binding energy region along the ΓK direction of the surface Brillouin zone (SBZ) are presented in Fig. 3a, while Fig. 3b shows the momentum distribution curves (MDCs) from the valence band maximum down to 0.94 eV below the VBM. We observe the expected valence band dispersion for multilayer MoS_2 in both samples.[28] In sample A, the valence band maximum is located at Γ 0.72 eV below the Fermi level, while in sample B it is at 0.90 eV (as accurately determined by extracting the corresponding spectra at the Γ point). This binding energy difference indicates that sample A experiences

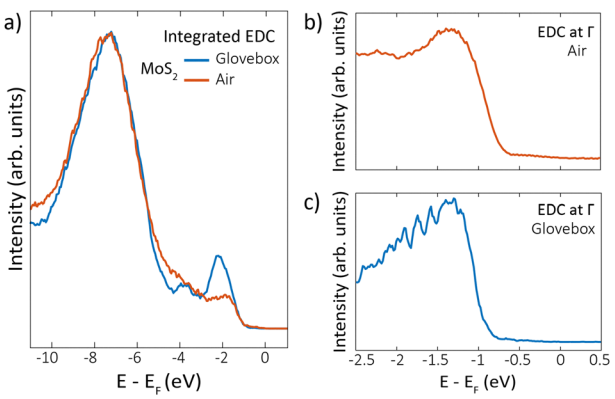

Fig. 2 Valence band for the air (red) and glove-box (blue) sample, taken in normal emission with 95 eV photon energy. (a) EDCs angle-integrated ~0.3 $Å^{-1}$ around the Γ point of the SBZ. (b) and (c) Angle-resolved EDCs taken at normal emission at Γ (0.07 $Å^{-1}$ acceptance).

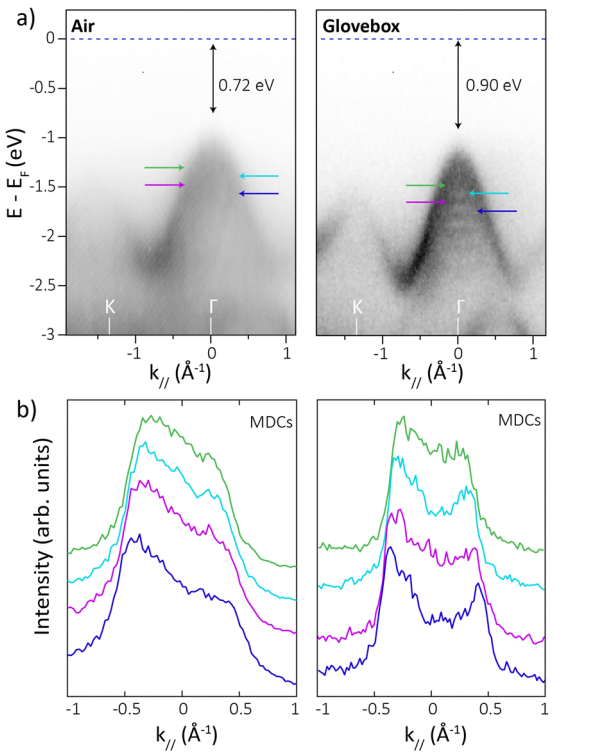

Fig. 3 (a) ARPES taken along the ΓK direction on the air (left) and glove-box (right) prepared samples. (b) MDCs taken at different BE values (−0.69 eV, −0.76 eV, −0.84 eV and −0.94 eV with respect to the VBM, from top to bottom) for the air-prepared (left) and glove-box protected (right) crystals.

a slight p-type doping. Traces of oxygen and carbon as main contaminants have been recently observed in air-exfoliated MoS_2,[29] as also disulfide and to minor extent Mo oxides were measured after 10 minutes exposure to air,[30] and similarly at edge or defect regions of chemically vapor deposited TMDs.[5] We can thus associate this slight p-type doping in the air-transferred crystal, mainly with oxygen contamination. On the other hand, sample A presents a long-term time stability of its electronic bands signal, as expected in the UHV environment.

The MDCs confirm these observations, clearly highlighting the main differences emerging between the air-exposed and glove-box/vacuum-prepared samples, as shown in Fig. 3b. Namely, sample A shows pronounced band broadening, whereas sample B displays well-defined bands. In particular, for the air-protected sample B, distinct side peaks are identifiable—arising from the intercept of the upper valence band at ± 0.35, ± 0.31, ± 0.27, and -0.22 Å^{-1} with corresponding binding energies of -0.94, -0.84, -0.76, and -0.69 eV below the VBM, respectively. From the electronic band dispersion and MDC analysis, the bandwidths along the ΓK direction are determined to be 1.08 ± 0.10 eV for sample B and 1.20 ± 0.10 eV for sample A, with effective hole masses $m_h^* = 1.6 \pm 0.1 m_e$ and $1.2 \pm 0.1 m_e$, respectively. These values are consistent with those reported for multilayer crystalline flakes.[31] The full-width at half-maximum of the bands, in the 1.0–2.2 eV BE range along the ΓK branch is reported in Fig. S1 of the SI. The width varies from ~ 0.45 Å^{-1} to ~ 0.30 Å^{-1} for sample A, while it changes from ~ 0.75 Å^{-1} to ~ 0.45 Å^{-1} for sample B, thus showing broader bands for the air-prepared sample. These differences between samples A and B can be attributed to surface air contamination[29,30] affecting the top-most MoS_2 layer, particularly the out-of-plane orbitals that mainly contribute to the upper band at low binding energies.

Conclusions

This study demonstrates the critical role of external perturbations in the electronic states of 2D TMD, in particular the importance of air protection in preserving the intrinsic electronic properties of exfoliated MoS_2 multilayers. An experimental micro-ARPES study revealed that MoS_2 samples prepared in a controlled, air-free environment exhibit a significantly higher spectral density of states and well-defined band structures. In contrast, air-prepared and transferred MoS_2 samples show broadened electronic states and slight p-doping, likely due to surface contamination, as evidenced by the evolution of the electronic bands associated with out of plane orbitals close to the valence band maximum.

Although ageing effects have been studied to be more effective on chemical vapour deposition (CVD) grown, than on exfoliated MoS_2,[9] our findings underscore that even for exfoliated MoS_2, known to be more stable than CVD-grown counterparts, maintenance of an inert atmosphere from cleavage to spectroscopic measurement is essential for obtaining an accurate representation of its very surface electronic structure. Our results on MoS_2 highlight the necessity of air-free preparation techniques for fundamental electronic state investigation of transition metal dichalcogenides and in general of cleavable 2D materials, useful for their potential applications in electronic and optoelectronic devices.

Author contributions

Dario Marchiani: data curation, formal analysis, investigation and methodology. Marta Pennese: data curation, formal analysis, investigation and writing – original draft. Nuria Jimenez-Arevalo, José Avila and Pavel Dudin: investigation. Maria Grazia Betti, Carlo Mariani and Riccardo Frisenda: conceptualization, funding acquisition, writing – original draft, writing – review and editing.

Conflicts of interest

There are no conflicts to declare.

Data availability

The data within this article will be made available from the corresponding authors upon reasonable request.

Supplementary information showing the full-width at half-maximum of the momentum distribution curves for both air-transferred and air-protected samples is available. See DOI: **https://doi.org/10.1039/d5tc01402f**

Acknowledgements

This work was supported by the PRIN Grants TUNES (2022NXLTYN), 2D-FRONTIERS (20228879FT), by European Union-Next Generation EU under PNRR-NEST project ENERGY SUSTAINABLE TRANSITION-NETWORK 4 Spoke 6 Next Generation EU-PE0000021, and by Sapienza Ateneo and ''Avvio alla ricerca'' funds.

Notes and references

1 L. Zhang and A. Zunger, *Nano Lett.*, 2015, **15**, 949.
2 K. F. Mak, C. Lee, J. Hone, J. Shan and T. F. Heinz, *Phys. Rev. Lett.*, 2010, **105**, 136805.
3 Y. Zhang, T.-R. Chang, B. Zhou, Y.-T. Cui, H. Yan, Z. Liu, F. Schmitt, J. Lee and R. Moore, *et al.*, *Nat. Nanotechnol.*, 2015, **9**, 111.
4 H. Yuan, Z. Liu, G. Xu, B. Zhou, S. Wu, D. Dumcenco, K. Yan, Y. Zhang and S.-K. Mo, *et al.*, *Nano Lett.*, 2016, **16**, 4738.
5 C. Kastl, R. J. Koch, C. T. Chen, J. Eichhorn, S. Ulstrup, A. Bostwick, C. Jozwiak, T. R. Kuykendall and N. J. Borys, *et al.*, *ACS Nano*, 2019, **13**, 1284.
6 A. M. van der Zande, P. Y. Huang, D. A. Chenet, T. C. Berkelbach, Y. M. You, G.-H. Lee, T. F. Heinz, D. R. Reichman, A. Muller and J. C. Hone, *Nat. Mater.*, 2013, **12**, 554.
7 F. Carrascoso, R. Frisenda and A. Castellanos-Gomez, *Nano Mater. Sci.*, 2022, **4**, 44–51.

8 E. Blundo, M. Felici, T. Yildirim, G. Pettinari, D. Tedeschi, A. Miriametro, B. Liu, W. Ma, Y. Lu and A. Polimeni, *Phys. Rev. Res.*, 2020, **2**, 012024.
9 J. Gao, B. Li, J. Tan, P. Chow, T.-M. Lu and N. Koratkar, *ACS Nano*, 2016, **10**, 2628.
10 A. O. Slobodeniuk and M. R. Molas, *Phys. Rev. B*, 2023, **108**, 035427.
11 X. Zheng, X. Miao, Y. Xiao, L. Guo, Y. Wang, T. Hu, X. Gong, C. Wu and C. Xiong, *Inorg. Chem. Front.*, 2022, **9**, 1785–1793.
12 B. S. Kim, J.-W. Rhim, B. Kim, C. Kim and S. R. Park, *Sci. Rep.*, 2016, **6**, 36389.
13 S. Guo, M. Luo, G. Shi, N. Tian, Z. Huang, F. Yang, L. Ma, N. Z. Wang, Q. Shi, K. Xu, Z. Xu, K. Watanabe, T. Taniguchi, X. H. Chen, D. Shen, L. Zhang, W. Ruan and Y. Zhang, *Rev. Sci. Instrum.*, 2023, **94**, 013903.
14 A. Grubišic-Cabo, M. Michiardi, C. E. Sanders, M. Bianchi, D. Curcio, D. Phuyal, M. H. Berntsen, Q. Guo and M. Dendzik, *Adv. Sci.*, 2023, **10**, 2301243.
15 I. Cucchi, I. Gutiérrez-Lezama, E. Cappelli, S. McKeown Walker, F. Y. Bruno, G. Tenasini, L. Wang, N. Ubrig, C. Line Barreteau, E. Giannini, M. Gibertini, A. Tamai, A. F. Morpurgo and F. Baumberger, *Nano Lett.*, 2019, **19**, 554.
16 M. Donarelli, F. Bisti, F. Perrozzi and L. Ottaviano, *Chem. Phys. Lett.*, 2013, **588**, 198.
17 T. Yanase, F. Uehara, I. Naito, T. Nagahama and T. Shimada, *ACS Appl. Nano Mater.*, 2020, **3**, 10462.
18 F. Margot, S. Lisi, I. Cucchi, E. Cappelli, A. Hunter, I. Gutiérrez-Lezama, K. Y. Ma, F. von Rohr, C. Berthod, F. Petocchi, S. Poncé, N. Marzari, M. Gibertini, A. Tamai, A. F. Morpurgo and F. Baumberger, *Nano Lett.*, 2023, **23**, 6433–6439.
19 E. Gao Enlai, S.-Z. Lin, Z. Qin Zhao, M. J. Buehler, X. Q. Feng and Z. Zu, *J. Mech. Phys. Solids*, 2018, **115**, 248–262.
20 M. Onodera, S. Masubuchi, R. Moriya and T. Machida, *Jpn. J. Appl. Phys.*, 2020, **59**, 010101.
21 A. Castellanos-Gomez, M. Buscema, R. Molenaar, V. Singh, L. Janssen, H. S. J. van der Zant and G. A. Steele, *2D Mater.*, 2014, **1**, 011002.
22 Q. Zhao, T. Wang, Y. K. Ryu, R. Frisenda and A. Castellanos-Gomez, *J. Phys. Mater.*, 2020, **3**, 016001.
23 P. Gant, F. Carrascoso, Q. Zhao, Y. K. Ryu, M. Seitz, F. Prins, R. Frisenda and A. Castellanos-Gomez, *2D Mater.*, 2020, **7**, 025034.
24 S. Khalid, B. Medasani, J. L. Lyons, D. Wickramaratne and A. Janotti, *2D Mater.*, 2024, **11**, 021001.
25 C. Lee, J. Hong, W. R. Lee, D. Y. Kim and J. H. Shim, *J. Solid State Chem.*, 2014, **211**, 113–119.
26 J. Yeh and I. Lindau, *At. Data Nucl. Data Tables*, 1985, **32**, 1–155.
27 M. D. Watson, M. Date, A. Louat and N. B. M. Schröter, *Phys. Rev. B*, 2024, **110**, L121121.
28 W. Jin, P.-C. Yeh, N. Zaki, D. Zhang, J. T. Sadowski, A. Al-Mahboob, A. M. van der Zande, D. A. Chenet and J. I. Dadap, *et al.*, *Phys. Rev. Lett.*, 2013, **111**, 106801.
29 P. F. Buitrago, S. Montoro, R. Vidal and F. Bonetto, *Vacuum*, 2024, **229**, 113586.
30 P. Afanasiev and C. Lorentz, *J. Phys. Chem. C*, 2019, **123**, 7486.
31 W. S. Yun, S. W. Han, S. C. Hong, I. G. Kim and J. D. Lee, *Phys. Rev. Lett.*, 2012, **85**, 033305.